Vol. 83 No. 4 pp. 724–732 ACTA GEOLOGICA SINICA Aug. 2009

Seismogenic Structure around the Epicenter of the May 12, 2008 Wenchuan Earthquake from Micro-seismic Tomography

AN Meijian[1, *], FENG Mei[1], DONG Shuwen[2], LONG Changxing[1], ZHAO Yue[1], YANG Nong[1], ZHAO Wenjin[2] and ZHANG Jizhong[1]

1 *Institute of Geomechanics, Chinese Academy of Geological Sciences, Beijing 100081, China*
2 *Chinese Academy of Geological Sciences, Beijing 100037, China*

Abstract: A three-dimensional local-scale *P*-velocity model down to 25 km depth around the main shock epicenter region was constructed using 83821 event-to-receiver seismic rays from 5856 aftershocks recorded by a newly deployed temporary seismic network. Checkerboard tests show that our tomographic model has lateral and vertical resolution of ~2 km. The high-resolution *P*-velocity model revealed interesting structures in the seismogenic layer: (1) The Guanxian-Anxian fault, Yingxiu-Beichuan fault and Wenchuan-Maoxian fault of the Longmen Shan fault zone are well delineated by sharp upper crustal velocity changes; (2) The Pengguan massif has generally higher velocity than its surrounding areas, and may extend down to at least ~10 km from the surface; (3) A sharp lateral velocity variation beneath the Wenchuan-Maoxian fault may indicate that the Pengguan massif's western boundary and/or the Wenchuan-Maoxian fault is vertical, and the hypocenter of the Wenchuan earthquake possibly located at the conjunction point of the NW dipping Yingxiu-Beichuan and Guanxian-Anxian faults, and vertical Wenchuan-Maoxian fault; (4) Vicinity along the Yingxiu-Beichuan fault is characterized by very low velocity and low seismicity at shallow depths, possibly due to high content of porosity and fractures; (5) Two blocks of low-velocity anomaly are respectively imaged in the hanging wall and foot wall of the Guanxian-Anxian fault with a ~7 km offset with ~5 km vertical component.

Key words: Wenchuan earthquake, seismogenic structure, micro-seismic tomography, Pengguan massif, Longmen Shan fault zone

1 Introduction

The Longmen Shan fault zone marks the steep basin-mountain transition between the Tibetan plateau in the west and the Sichuan basin in the east (Figure 1). The fault zone is characterized by a NE strike and composed of three major faults: Wenchuan-Maoxian fault in the northwest, Yingxiu-Beichuan-Qingchuan fault in the central and Guanxian-Anxian fault in the southeast. The outcrops between the Wenchuan-Maoxian and Yingxiu-Beichuan faults in the study area (Figure 1) are Proterozoic igneous Pengguan massif composed of diorites and granites, and the other areas are mainly covered by sedimentary rocks from Proterozoic era. The outcrops of the sedimentary rocks are older towards the Pengguan massif. The geological features around the Pengguan massif indicated that the old and deep rocks have been taken up to the surface by the thrust of the Wenchuan-Maoxian and Yingxiu-Beichuan faults. Thus, the Wenchuan-Maoxian and Yingxiu-Beichuan faults could be taken as the boundary faults between the Tibetan plateau and Sichuan basin, while the Guanxian-Anxian fault occurs within the Sichuan Basin.

Most study results around the Longmen Shan fault zone before 2008, e.g., relatively small lateral GPS movement rate (e.g., Zhang et al., 2004), are supportive for the faults are seismically safer than the Xianshuihe faults to the south. However, the M_S 8.0 Wenchuan earthquake on May 12, 2008 (as the epicenter is in the Wenchuan county, hereinafter, we term it as Wenchuan earthquake) exactly occurred in the southern tip of the Pengguan massif close to the junction of the Wenchuan-Maoxian and Yingxiu-Beichuan faults (Figure 1), and this earthquake is so strong that it triggered hundred kilometers of tectonic activity along the fault system. The occurrence of the Wenchuan

* Corresponding author. E-mail: meijianan@yahoo.com.cn

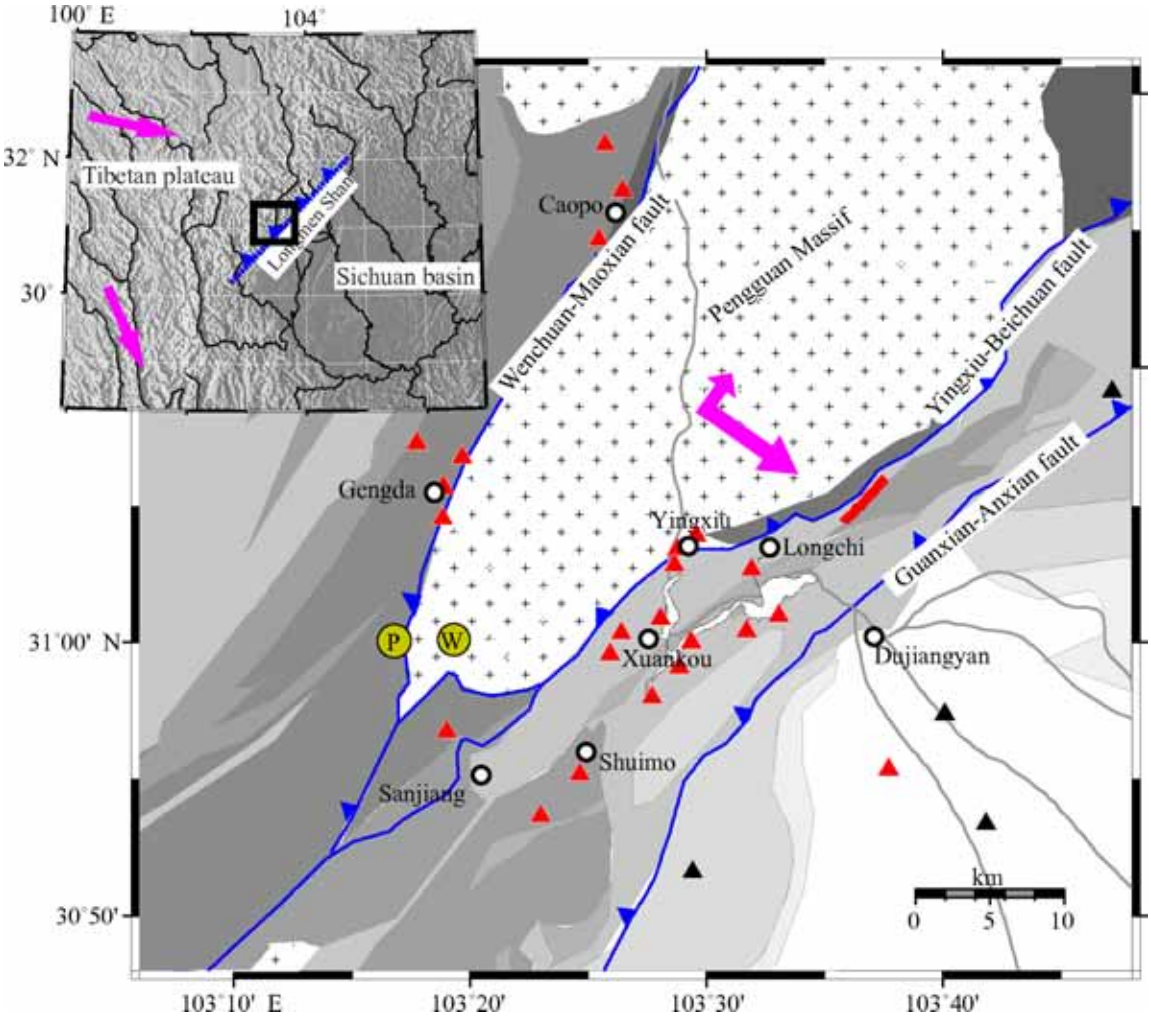

Fig. 1. Geographical and geological sketch map of the study area.

The inset map shows the surrounding tectonic settings of the study area (rectangle). The geological information was simplified from State Expert Committee of the Wenchuan Earthquake (2008). The areas filled with plus symbols are igneous rocks, and the other areas are sedimentary rocks. The sedimentary rocks with young to old ages are shaded by white to gray colors. Red triangles are seismic stations used here, black triangles are seismic stations of China Earthquake Administration; gray circles marked by "W" and "P" are hypocenter of the Wenchuan earthquake respectively from the WHDF catalog and from An et al. (2009); blue lines are the Longmen Shan fault zone; gray lines are rivers, and white areas close to Yingxiu town represent the Zipingpu reservoir; thick red segment denote the escarpment position in the Shenxigou valley formed by the main shock rupture; purple thick arrows on the hanging wall of the Yingxiu-Beichuan fault marks the fault movement components, and the arrows in the inset map mark the movement of the eastern Tibetan plateau.

earthquake implied that the Longmen Shan fault zone was not sufficiently studied prior to the occurrence of the Wenchuan earthquake.

Immediately after the occurrence of the Wenchuan earthquake, field measurements of surface ruptures and co-seismic deformations were made (e.g., Chen et al., 2008; Dong et al., 2008a; Dong et al., 2008b; Ma et al., 2008) and indicated that co-seismic deformations are different in different parts along the Longmen Shan fault zone. The co-seismic deformation in the Yingxiu-Beichuan part of the Longmen Shan fault zone close to the epicenter is a northeast-striking northwest-dipping thrust with small right-lateral strike-slip component, while in the Beichuan-Qingchuan part in the north the deformation is obviously right-lateral strike-slip with a small thrust component. Such field observations are important to reveal the superficial attribute of the faults. Seismic receiver function and regional-scale body-wave tomographic analysis (e.g., Liu et al., 2008) obtained valuable information on the Moho discontinuity and crustal seismic velocities beneath the Longmen Shan fault zone. However, to further understand the earthquake itself, it is necessary to extract high-resolution information on the seismogenic layer above 25 km in depth. Due to the large distance from the seismic stations to the main shock and large inter-station distances used in the previous studies (e.g., Liu et al., 2008), their regional-scale models with lateral resolution worse than 10 km can hardly have reliable structure information inside the

complex seismogenic layer beneath the Longmen Shan fault zone. Therefore, to fill the gap between the in-site geological investigations made on the earth's surface and regional-scale geophysical explorations of crust and lithosphere, it is necessary to carry out a high-resolution local-scale study to reveal the upper crust structures and their possible connections with seismicity around the main shock epicenter.

The goal of the present study is to give the 3-D upper-crustal *P*-velocity structures in local scale around the Wenchuan earthquake hypocenter by high-resolution micro-seismic tomography using seismic records of 26 seismic stations deployed after the occurrence of the Wenchuan earthquake, and then to show deep tectonic information extracted according to the possible connections among *P*-velocity anomalies, structure and seismicity.

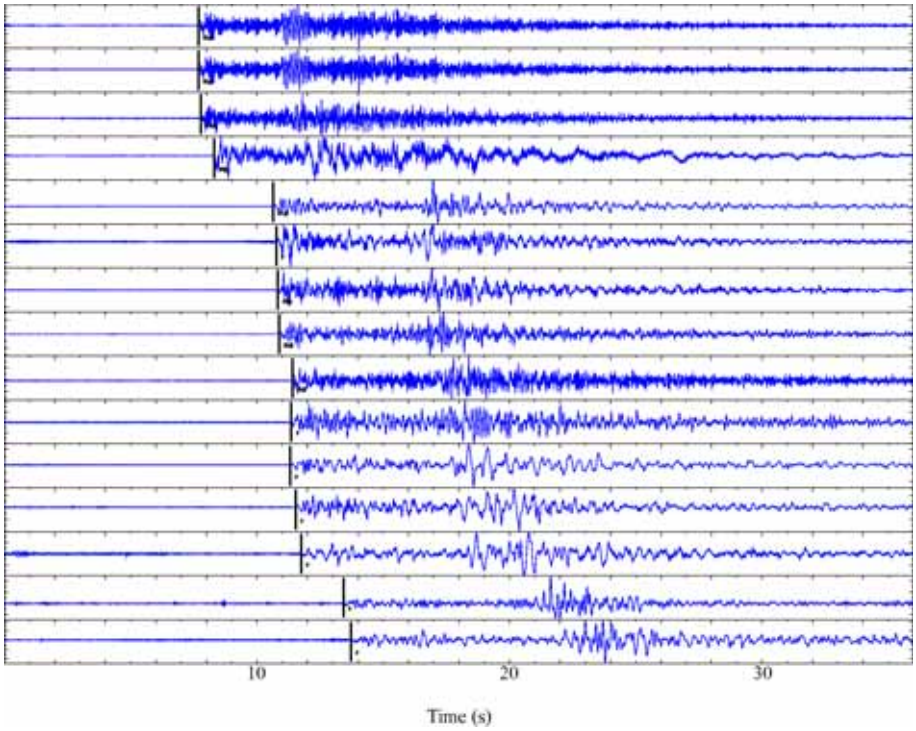

Fig. 2. Example of vertical-component seismic waveforms of one aftershock simultaneously recorded by our 15 stations.
The black bar in each subfigure indicates *P* phase position.

2 Aftershock Observations

To investigate the seismic structures around the main shock epicentral region in detail, we deployed 26 seismic stations (red triangles in Figure 1), which are equipped with short-period Mark Products (Sercel) L-22D sensors and Reftek digitizers after the earthquake occurred. Unlike mostly-used broadband sensors with flat frequency response at lower frequencies, the sensor of L-22D has flat frequency response for frequencies higher than ~4 Hz, which is suitable for high-frequency micro-seismic study. Figure 1 also shows the seismic stations around the study area deployed by the China Earthquake Administration (CEA) (black triangles in Figure 1). The CEA seismic stations have relatively large inter-station distances and are equipped with broadband sensors. Though our seismic stations are not evenly distributed in the study area due to the difficulties on transportation, the spacing between our seismic stations is much smaller than that between the CEA stations and the Zipingpu Reservoir seismic network, which only includes 7 stations around the Zipingpu Reservoir. Our densely-distributed seismic stations will, hopefully, result in a high resolution local-scale seismic structure model.

The three-dimensional upper-crustal *P*-velocity model of the present study is constructed by seismic tomographic inversion of *P*-wave travel time observations. To obtain the *P*-wave travel time, the following major data processing procedures are required: (1) automatically trigger seismic events and slice the event waveforms from the continuous raw seismic data; (2) manually mark/pick the first arriving *P*-wave phases for the triggered events; and (3) determine event origin time and hypocenter location for the triggered events. Figure 2 shows an example of seismic waveforms of one event recorded by our seismic stations. From this figure we can see that the seismic waveforms used here are of high signal-to-noise ratio and have clear onset of *P*-wave phase which ensure a good data condition.

The *P*-wave travel time data used in this study were analyzed by An et al. (2009) who retrieved deep ruptures around the hypocenter of the 2008 Wenchuan Earthquake from aftershock observations. To improve the reliability of the hypocenter determination, only events simultaneously recorded by at least 10 stations were considered. The earthquakes were preliminarily located using the program hypo71 (Lee and Lahr, 1972) and then relocated using a 3-D grid-search inversion on the basis of wave-propagation forward modeling by finite-difference calculation (Vidale, 1988, 1990). As aftershocks of a strong main shock are normally very abundant, An et al. (2009) only processed 108-days of seismic data from July to October of 2008, they

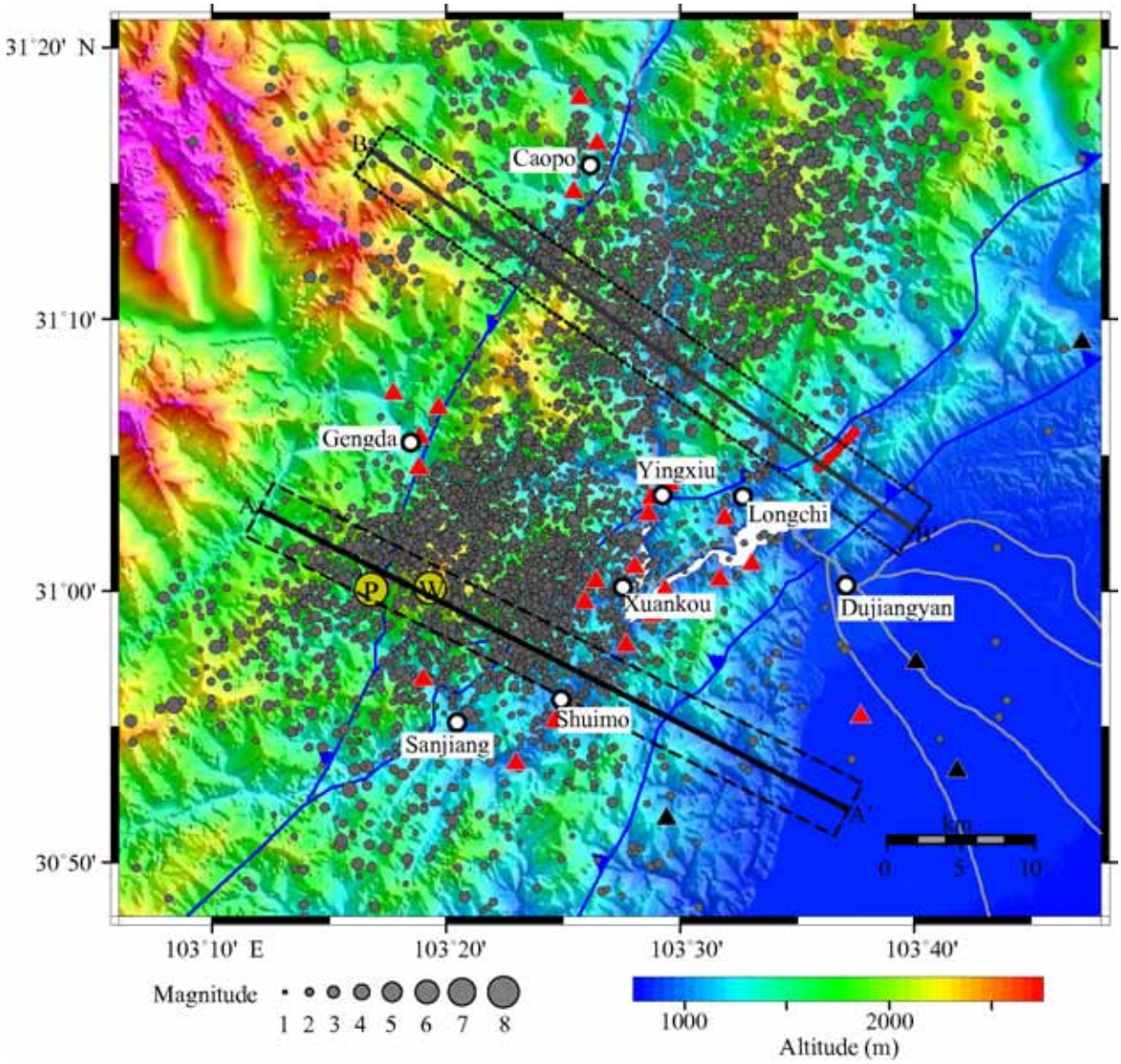

Fig. 3. Distribution of aftershocks (gray-circles scaled with magnitude) used in the present study.
Solid lines labeled with AA' and BB' are locations of two transects to be shown in Figure 4. Dashed rectangles denote the 2-km-projection area from the central transect line. The others are the same as in Figure 1.

finally retrieved 5856 aftershocks that are enough for the requirement of the present micro-seismic tomographic study. As each aftershock is recorded by more than 10 stations, we obtained a total of 83821 *P*-wave travel time observations (or 83821 event-to-receiver seismic rays beneath the study region). Such a large dataset gives a very good spatial ray sample of our study area.

Figure 3 shows the seismic stations and micro-earthquakes used in the present study. Since the aftershocks are mostly located along the Longmen Shan fault zone and their focal depths are generally less than ~20 km, we defined our study region as a 3-D cube of 88 km in x (east-west), 88 km in y (north-south) and 25 km in z (depth) direction with an approximate geographic center in the Yingxiu town. As the depth of ~20 km is the base of the upper crust along the Longmen Shan fault zone (Zhao et al., 1997; Bassin et al., 2000), our resulting tomographic model mainly reflects the upper-crustal *P*-velocity structure of the study area.

3 Method

Similar to the basic theory of medical Computerized Tomography (CT) that utilizes *X*-rays imaging body to find the infection focus, seismic tomography is a geophysical method that utilizes seismic-rays imaging the Earth interior structures to find seismic velocity anomaly. Since it appeared in 1974 (Aki et al., 1974), the seismic tomography has been widely applied in global- and regional-scale earth's structure studies (van der Hilst et al., 1991;

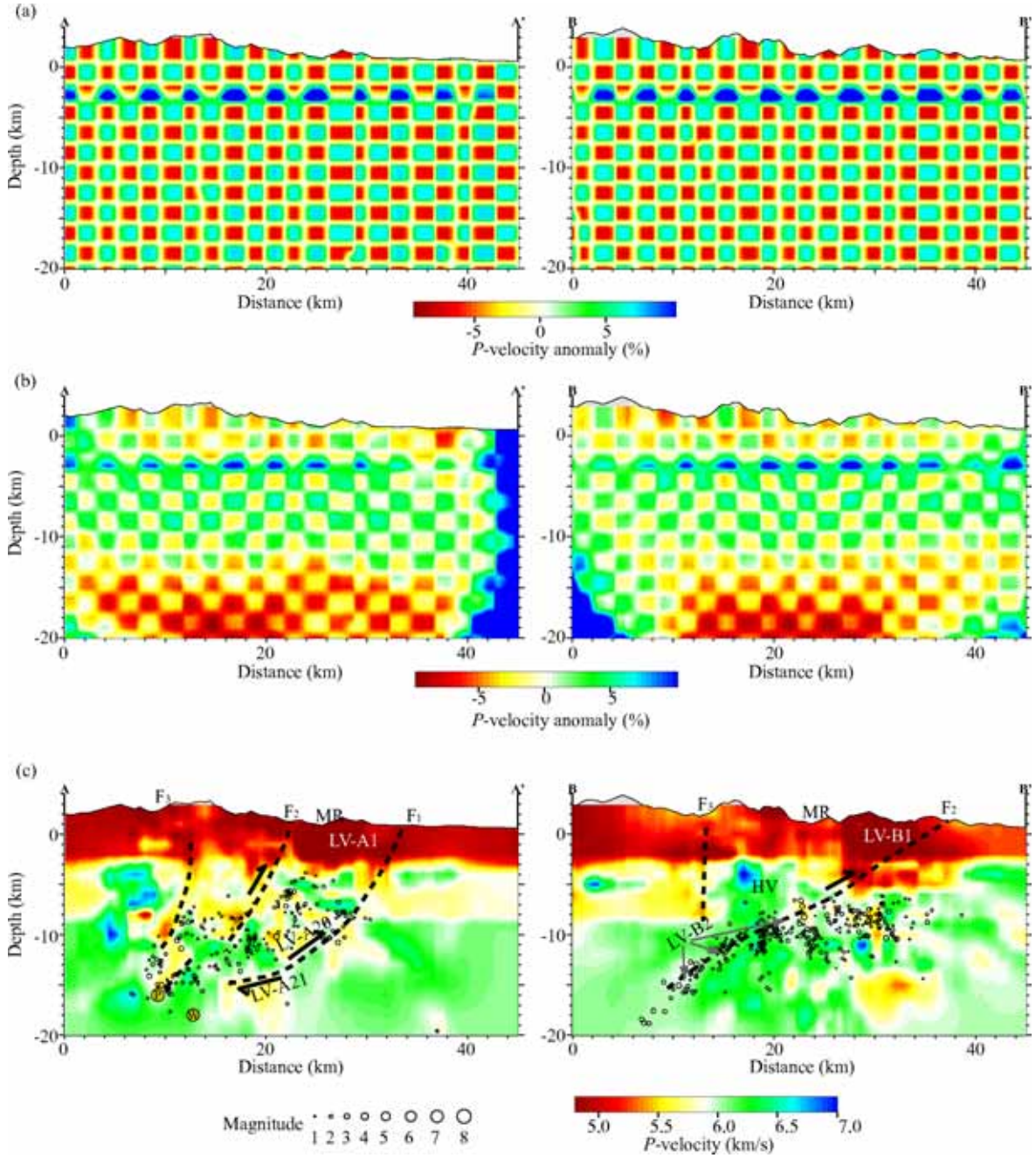

Fig. 4. Two vertical transects through the final *P*-velocity model (c) together with its checkerboard test input model (a) and retrieved model (b).

Aftershocks inside the dashed rectangular area denoted in Figure 3 are projected on the central transect line.

Bijwaard et al., 1998; van der Voo et al., 1999; Schimmel et al., 2003). There are also many tomographic studies (e.g., Liu et al., 1991; Xu et al., 2002; Huang and Zhao, 2004; Lei and Zhao, 2005; Zhou and Murphy, 2005; Huang and Zhao, 2006; Li et al., 2006; Lei et al., 2008) that revealed important deep structure features beneath different regions of China. However, it was seldom applied in high-resolution local-scale studies. Wang et al. (2006) firstly introduced the micro-seismic tomography method into a local-scale study of oil fields in the Qaidam basin in China. Later, the method was greatly improved in the computation resolution and efficiency (Feng et al., 2007), and consequently becomes more suitable for a high-resolution local-scale tomographic study.

According to the seismic-wave propagation theory, travel time for the *i*-th seismic wave from hypocenter to station/receiver (T_i) can be considered as integral of travel time along the seismic ray path ($\int_{receiver}^{hypocenter} dt$).

For computing simplification, the study region is discretized as many small cubes. Supposing that each small cube has homogeneous/fixed *P*-wave velocity (α), thus the travel time integral along seismic ray becomes travel time summation ($\Sigma\Delta t$) in all the discretized cubes and can be expressed as (Wang et al., 2006):

$$T_i = \sum_{j=0}^{n} \Delta t_j = \sum_{j=0}^{n} \frac{\Delta l_j}{\alpha_j} \quad ,$$

where, T_i is the observational travel time for the *i*-th seismic ray and the subscript *i* varies from one to the maximum seismic ray numbers (*m*, here is 83821); Δl_j is the ray segment length in the *j*-th discretized small cube crossed by the seismic wave and the subscript *j* varies from one to the maximum cube numbers (*n*); α_j is the *P*-velocity of the *j*-th small cube. In the above equation, T_i is observed data, Δl_j can be obtained by seismic ray tracing from the hypocenter to the receiver. Thus only the *P*-velocity of each cube α_j is unknown. The above equation represents the travel time for one seismic wave ray. For all seismic rays, we constructed many such travel time equations, the unknown *P*-velocities can then be determined using a linear inversion method (Paige and Saunders, 1982a, b).

One of the key points that influences the resolution of the final results is the choice of the ray tracing method, or the method of calculating Δl_j. Most global- or regional-scale studies normally used the shooting or bending ray tracing methods which are more efficient but less precise (Rawlinson and Sambridge, 2003). Here we used wave-front ray tracing method (Vidale, 1988, 1990) which requires great computing efforts but results in higher resolution wave propagation. In the present study, we parameterized our study region by 0.5 km of inter-cube space (i.e., the size of each discretized cube is 0.5×0.5×0.5 km^3). However, as tomographic inversion problem is often ill-posed, *a priori* constraints are required to stabilize the inversion. We introduce lateral and vertical model smoothing as regularization to result in a more physically-reasonable structure model.

A checkerboard test is a helpful tool to indicate the spatially varying resolving power of seismic tomography. Figure 4a, b shows the checkerboard test results using the same path coverage as that in constructing our final tomographic model. The *P*-velocity perturbations of the checkers are assigned as ±7% relative to the reference model. The inverted model of the checkerboard tests retrieved checkers with a size of 2 km in both lateral and vertical directions in most study areas (Figure 4a, b). Thus the average lateral and vertical resolution length in our central study area is ~2 km, while the resolving power weakens in the marginal regions.

4 Results and Discussions

The *P*-velocities from micro-seismic tomography are displayed as vertical transects across two different parts of the Longmen Shan fault zone. Figure 3 shows the location of the two transects. Their correspondent *P*-velocities together with aftershock hypocenters are shown in Figure 4c. The hypocenters projected on the *P*-velocity transects in Figure 4c were clustered aftershocks (An et al., 2009) processed using a relative relocation method hypoDD but not those relocated using a wave-front modeling method in the present study. The hypoDD method (Waldhauser and Ellsworth, 2000) is suitable for detecting deep rupture geometry but tends to put close-events together and causes over-concentrated aftershocks in certain areas. Such over-concentrated aftershocks may bias seismic velocity structure in a tomographic inversion. Therefore, we did not directly use hypocenters relocated by An et al. (2009) in our tomographic inversion. However, to correlate *P*-velocity anomaly with deep seismic rupture geometry, we showed our *P*-velocities together with the aftershocks (An et al., 2009) relocated by the hypoDD method in Figure 4c. Topography correction is considered for the hypocenters in Figure 4c.

Transect AA' crosses through the Wenchuan earthquake hypocenter region in the southwestern study area in NWW-SEE direction, and is approximately perpendicular to the Longmen Shan fault zone (Figure 3). At depths (relative to surface) smaller than ~5 km, obvious low velocities (marked as LV-A1 in Figure 4c) are shown beneath the Minjiang River (MR) on the transect AA' (Figure 4c), while normal to relatively higher velocities are observed beneath the Pengguan massif bounded by the Wenchuan-Maoxian fault (F_3) and the Yingxiu-Beichuan fault (F_2). At greater depths, most clustered aftershocks locate in high-velocity areas that are bounded by a nearly vertical low-velocity belt beneath the Wenchuan-Maoxian fault (delineated as dashed line beneath F_3) and by a NW dipping low-to-high velocity boundary (delineated as dashed lines) beneath the Guanxian-Anxian fault (F_1). In between, there is another subtle low-to-high velocity boundary (marked as dashes) beneath the Yingxiu-Beichuan fault (F_2). If these dashes marked in the transect AA' (Figure 4c) reflect the three faults of the Longmen Shan fault zone, then they have increasingly steep occurrence from the basin side to the mountain side and from deep to the Earth's surface.

The hypocenter of the Wenchuan earthquake according to the WHDF (Weekly Hypocenter Data File) earthquake catalog from USGS marked as "W" in the transect (Figure 4c) locates in the high velocity area between F_1 and F_2. As the hypocenter represents the position where the earthquake initiated, the Wenchuan earthquake should

initiate from the foot wall of F_2 which is quite unrealistic. An et al. (2009) proposed a slightly different hypocenter location for the Wenchuan earthquake based only on aftershock analysis. Their proposed hypocenter (marked as "P") at the deep end of the clustered aftershocks locates at the low-to-high velocity boundary reflecting the Yingxiu-Beichuan fault (F_2), at the deep end of the vertical low-velocity belt beneath F_3 reflecting the Wenchuan-Maoxian fault or the western boundary of the Pengguan massif, and at the extrapolation of the interpreted deep Guanxian-Anxian fault (dashed lines close to labels LV-A20 and LV-A21 in the Figure 4c). The correlation between the proposed hypocenter from aftershock clusters and the interpreted faults from seismic-velocity anomaly pattern confirms that the proposed Wenchuan earthquake hypocenter location is more reasonable than that determined using global seismic networks in the WHDF catalog and that the Yingxiu-Beichuan fault is the main rupture fault of the Wenchuan earthquake.

Along the indicative dashed line of the Guanxian-Anxian fault, two blocks of low-velocity anomaly (LV-A20 and LV-A21 on transect AA') are respectively imaged in the hanging wall and foot wall of the Guanxian-Anxian fault with a ~7 km offset along the fault plane with ~5 km vertical component. If the offsets were caused by accumulative thrust displacement along the fault during the uplift of the Tibetan plateau, an ~0.5 km/Ma thrust rate and ~0.3 km/Ma uplift rate might exist along the Guanxian-Anxian fault since the eastern Tibetan plateau started uplifting ~15 Ma ago when the Longmen Shan fault zone became active (Arne et al., 1997; Kirby et al., 2002; Clark et al., 2005; Burchfiel et al., 2008).

Transects BB' mainly crosses through the igneous Pengguan massif in the northeastern study area in NW-SE direction, and is also approximately perpendicular to the Longmen Shan fault zone (Figure 3). A co-seismic thrust escarpment extending for several kilometers was found in the Shenxigou valley close to the Yingxiu-Beichuan fault (marked as a red bar in Figure 3). Striking features on transect BB' include the upwarping high velocities (HV on transect BB' in Figure 4c) above the NW dipping aftershock cluster between the Wenchuan-Maoxian fault (F_3) and the Minjiang River (MR) and the very low velocities down to ~8 km (LV-B1) around the outcrop of the Yingxiu-Beichuan fault. Besides, a narrow belt of normal-to-low velocity (LV-B2) can be traced along the NW dipping aftershock cluster.

As aftershocks frequently occur along/around the main shock rupture plane, the NW dipping aftershock cluster on transect BB' may reflect the occurrence of the main shock rupture plane. The extrapolation of the aftershock cluster (dashed line) shows up around the Yingxiu-Beichuan fault (F_2), confirming that the Yingxiu-Beichuan fault is the main rupture fault of the Wenchuan earthquake (An et al., 2009). Thus, our imaged upwarping high velocities HV on transect BB' should lie within the hanging wall of the Yingxiu-Beichuan fault. As seismic velocity normally increases with depths due to increasing content of high-density minerals or high-pressure metamorphic materials, the higher velocities in the hanging wall compared with the foot wall at the same depths are quite possibly associated with the upward thrust movement of the hanging wall of the Yingxiu-Beichuan fault. On the northwest side of the high velocity HV in the transect BB', there is an obvious low velocity anomaly down to the depth position of ~8 km bounded by a nearly vertical limit beneath the Wenchuan-Maoxian fault. Such structural features possibly indicate that the occurrence of the Wenchuan-Maoxian fault is nearly vertical and that the velocities beneath the Pengguan massif are higher than these west of the Wenchuan-Maoxian fault. On this viewpoint, the Pengguan massif may extend down to at least ~8 km and have 10 km of thickness if the elevation is considered.

The very low velocities LV-B1 in the shallow depths covered a large area between the Minjiang River and the Yingxiu-Beichuan fault, where also the long co-seismic Shenxigou escarpment was found. Considering that LV-B1 also locates around the end of the extrapolation of the aftershock cluster belt, the thrust movement of the Yingxiu-Beichuan fault should finally concentrate at shallow depths in the LV-B1 area. As porosity and cracks/fractures in shallow depths can strongly decrease the seismic velocities of sediments or rocks, the effects of high porosity and cracks/fractures caused by the tectonic activity should be main cause of the very low velocity anomaly around the Yingxiu-Beichuan fault. Stresses in the shallow saturated sediments or in the fractured rocks with small strength are easily released before they accumulate to be large enough for a brittle earthquake. That can explain why there are fewer aftershocks in the shallow depths around the LV-B1 area than in greater depths, though LV-B1 covers part of the main shock rupture. The area around the label LV-A1 in the transect AA' (Figure 4c) has similar low seismicity and very-low velocity to that around LV-B1 in the transect BB'. Thus, they could also be associated with high porosity and high crack density.

Different from the very low velocities at shallow depths caused by high content of porosity or fractures, we did not find prominent low velocities at depths greater than ~5 km along the main rupture plane in the transect BB'. Possibly because the Yingxiu-Beichuan fault is compressive thrust and the static pressure below ~5 km depth becomes high enough to close the crack porosity (Christensen, 1996), the seismic velocities are less affected by the effects of high

porosity and fractures. However, a narrow belt of normal-to-low velocity is visible along the rupture plane (marked as LV-B2 on transect BB' in Figure 4c). Such weak low velocity anomaly is possibly related to unconsolidated materials along the rupture plane resulting from the mainshock and aftershocks, which can slightly slow down seismic wave speed. Furthermore, rupture friction and high thermal conductivity in the fractured materials can cause temperature to increase and thus velocity to decrease in/around the rupture plane.

5 Conclusions

To investigate the three-dimensional structure in seismogenic layer around the Wenchuan earthquake main shock region, we constructed a densely distributed seismic network of 26 short-period seismometers around the epicenter after the earthquake occurred. Using the abundant seismic travel-time observations, a three-dimensional local-scale *P*-velocity model down to 25 km depth around the main shock epicenter region was constructed by a local-scale micro-seismic tomographic inversion based on finite-differential wave-front ray-tracing method. Checkerboard tests show that our tomographic model has lateral and vertical resolution of ~2 km, which is much better than previous regional scale tomographic models. The high-resolution *P*-velocity model showed strongly heterogeneous seismogenic structures around the Wenchuan earthquake hypocenter region. From these seismogenic structures, some deep tectonic information was extracted.

The Guanxian-Anxian, Yingxiu-Beichuan and Wenchuan-Maoxian faults are well delineated by sharp velocity changes. Beneath the Wenchuan-Maoxian fault, the western boundary of Pengguan massif, a sharp lateral velocity variation is found, possibly indicating the fault's plane is vertical. On this viewpoint, the hypocenter of the Wenchuan earthquake should locate at the conjunction point of the Yingxiu-Beichuan, Wenchuan-Maoxian, Guanxian-Anxian faults and the NWW-SEE potential fault proposed by an aftershock clusters study (An et al., 2009). Along the main shock deep rupture, the Yingxiu-Beichuan fault plane, a narrow belt of normal-to-low velocity is visible. The slight low velocity may be caused by unconsolidated materials along the rupture plane resulted from the earthquake, or by a slightly high temperature caused by rupture friction and high conductivity in the unconsolidated materials in the rupture plane. Two blocks of low-velocity anomalies are respectively imaged in the hanging wall and foot wall of the Guanxian-Anxian fault with a ~7 km offset along the fault plane with ~5 km vertical component.

The Pengguan massif has generally higher velocity than its surrounding areas, and may extend down to at least 10 km from the surface. Most clustered aftershocks and the main shock hypocenter from WHDF locate in high-velocity areas, however, the main shock hypocenter proposed from aftershock clusters locates at the low-to-high velocity boundary along the Yingxiu-Beichuan fault plane. The areas close to the main shock rupture outcrop, e.g., Shenxigou valley, have a low velocity and low seismicity in the shallow depths. The low velocity and low seismicity close to the main-shock rupture outcrop may indicate that the area is totally cracked down to 8 km deep.

Acknowledgements

Financial support was given by the Basic Research Foundation of the Institute of Geomechanics, CAGS (grant DZLXJK200707) and Natural Science Foundation of China (grant 40674058). All figures in this article were produced using the Generic Mapping Tool (Wessel and Smith, 1991).

Manuscript received April 24, 2009
accepted May 25, 2009
edited by Jiang Shaoqing

References

Aki, K., Christoffersson, A., Husebye, E.S., et al., 1974. Three-dimensional seismic-velocity anomalies in the crust and upper-mantle under the U.S.G.S. California seismic array (abstract). *EOS Trans. AGU.*, 56: 1145.

An Meijian, Feng Mei and Long Changxing, 2009. Deep ruptures around the hypocenter of the 2008 Wenchuan earthquake implied from aftershock observations. *Tectonophysics*, submitted.

Arne, D., Worley, B., Wilson, C., Chen Shefa, Foster, D., Luo Zhili, Liu Shugen and Dirks, P., 1997. Differential exhumation in response to episodic thrusting along the eastern margin of the Tibetan Plateau. *Tectonophysics*, 280(3–4): 239–256.

Bassin, C., Laske, G. and Masters, G., 2000. The current limits of resolution for surface wave tomography in North America. *EOS Trans. AGU.*, 81: F897.

Bijwaard, H., Spakman, W. and Engdahl, E.R., 1998. Closing the gap between regional and global travel time tomography. *J. Geophys. Res.*, 103(B12): 30055–30078.

Burchfiel, B.C., Royden, L.H., van der Hilst, R.D., Hager, B.H., Chen, Z., King, R.W., Li, C., Lü, J., Yao, H., and Kirby, E., 2008. A geological and geophysical context for the Wenchuan earthquake of 12 May 2008, Sichuan, People's Republic of China. *GSA Today*, 18(7): 4–11.

Chen Guihua, Xu Xiwei, Zheng Rongzhang, Yu Guihua, Li Feng, Li Chenxia, Wen Xueze, He Yulin, Ye Youqing, Chen Xiancheng and Wang Zhicai, 2008. Quantitative analysis of the co-seismic surface rupture of the 2008 Wenchuan earthquake, Sichuan,China along the Beichuan-Yingxiu fault. *Seismol. Geol.*, 30(3): 723–737 (in Chinese with English abstract).

Christensen, N.I., 1996. Poisson's ratio and crustal seismology. *J. Geophys. Res.*, 101(B2): 3139–3156.

Clark, M.K., House, M.A., Royden, L.H., Whipple, K.X, Burchfiel, B.C., Zhang, X., and Tang, W., 2005. Late Cenozoic uplift of southeastern Tibet. *Geology*, 33(6): 525–528.

Dong Shuwen, Zhang Yueqiao, Long Changxing, Wu Zhenhan, An Meijian, Zhang Yongshuang, Yang Nong, Chen Zhengle, Lei Weizhi, Shi Wei and Shi Jusong, 2008a. Surface rupture investigation of the Wenchuan M_S 8.0 earthquake of May 12th, 2008, West Sichuan, and analysis of its occurrence setting. *Acta Geoscientica Sinica*, 29(3): 392–396 (in Chinese with English abstract).

Dong Shuwen, Zhang Yueqiao, Wu Zhenhan, Yang Nong, Ma Yinsheng, Shi Wei, Chen Zhengle, Long Changxing and An Meijian, 2008b. Surface rupture and co-seismic displacement produced by the M_S 8.0 Wenchuan earthquake of May 12th, 2008, Sichuan, China: eastwards growth of the Qinghai-Tibet plateau. *Acta Geologica Sinica* (English Edition), 82(5): 938–948.

Feng Mei, An Meijian, Wang Xiaofeng, Ma Yinsheng, Jiang Rongbao and Li Li, 2007. Micro-earthquakes in Shizigou and their geological significances. *J. Geomechanics*, 13(2): 173–178.

Huang Jinli and Zhao Dapeng, 2004. Crustal heterogeneity and seismotectonics of the region around Beijing, China. *Tectonophysics*, 385: 159–180.

Huang Jinli and Zhao Dapeng, 2006. High-resolution mantle tomography of China and surrounding regions. *J. Geophys. Res.*, 111(B9): B09305.

Kirby, E., Reiners, P.W., Krol, M.A., Whipple, K.X., Hodges, K. V., Farley, K.A., Tang Wenqing and Chen Zhiliang, 2002. Late Cenozoic evolution of the eastern margin of the Tibetan Plateau:Inferences from $^{40}Ar/^{39}Ar$ and (U-Th)/He thermochronology. *Tectonics*, 21(1): 1001.

Lee, W.H.K., and Lahr, J.C., 1972. HYPO71: A computer program for determining hypocenter, magnitude, and first motion pattern of local earthquakes (U.S. Geol. Surv. Open-File Rep.).

Lei Jianshe and Zhao Dapeng, 2005. P-wave tomography and origin of the Changbai intraplate volcano in Northeast Asia. *Tectonophysics*, 397: 281–295.

Lei Jianshe, Xie Furen, Lan Congxin, Xing Chengqi and Ma Shizhen, 2008. Seismic images under the Beijing region inferred from P and PmP data. *Phys. Earth Planet. Ints.*, 168(3–4): 134–146.

Li Zhiwei, Xu Yi, Hao Tianyao and Liu Jinsong, 2006. Seismic tomography and velocity structure in the crust and upper mantle around Bohai Sea area. *Chinese J. Geophys.*, 49(3): 797–804 (in Chinese with English abstract).

Liu Futian, Wu Hua, Liu Jianhua, Hu Ge, Li Qiang and Qu Kexin, 1991. 3-D velocity images beneath the Chinese continent and adjacent regions. *Geophys. J. Int.*, 101: 379–394.

Liu Qiyuan, Chen Jiuhui, Li Shuncheng, Li Yu, Guo Biao, Wang Jun and Qi Shaohua, 2008. The M_S 8.0 Wenchuan Earthquake: Preliminary Results from the Western Sichuan Mobile Seismic Array Observations. *Seismol. Geol.*, 30(3): 584–596 (in Chinese with English abstract).

Ma Yinsheng, Long Changxing, Tan Chengxuan, Wang Tao, Zhang Yongshuang, Lei Weizhi, Li Bin, Gong Mingquan, Liao Chunting and Wu Manlu, 2008. Co-seismic deformation features and segmentation of the M_S 8.0 Wenchuan earthquake in Sichuan, China. *Geol. Bull. China*, 27(12): 2076–2085 (in Chinese with English abstract).

Paige, C.C., and Saunders, M.A., 1982a. LSQR: An algorithm for sparse linear equations and sparse least squares. *ACM Trans. Math. Softw.*, 8(2): 43–71.

Paige, C.C., and Saunders, M.A., 1982b. Algorithm 583, LSQR: Sparse linear equations and least squares problems. *ACM Trans. Math. Softw.*, 8(2): 195–209.

Rawlinson, N., and Sambridge, M., 2003. Seismic traveltime tomography of the crust and lithosphere. *Adv. Geophys.*, 46: 81–197.

Schimmel, M., Assumpção, M.S., and VanDecar, J.C., 2003. Seismic velocity anomalies beneath SE Brazil from P and S wave travel time inversions. *J. Geophys. Res.*, 108(B4): 2191.

State Expert Committee of the Wenchuan Earthquake, 2008. Atlas of earthquake and geological disasters for the Wenchuan earthquake. SinoMaps Press, Beijing (in Chinese).

Van der Hilst, R.D., Engdahl, E.R., Spakman, W., and Nolet, G., 1991. Tomographic imaging of subducted lithosphere below northwest Pacific island arcs. *Nature*, 353: 37–42.

Van der Voo, R., Spakman, W. and Bijwaard, H., 1999. Tethyan subducted slabs under India. *Earth Planet. Sci. Lett.*, 171: 7–20.

Vidale, J.E., 1988. Finite-difference calculation of travel times. *Bull. Seismol. Soc. Am.*, 78(6): 2062–2076.

Vidale, J.E., 1990. Finite-difference calculation of travel times in three dimensions. *Geophysics*, 55(5): 521–526.

Waldhauser, F., and Ellsworth, W.L., 2000. A double-difference earthquake location algorithm: method and application to the Northern Hayward Fault, California. *Bull. Seismol. Soc. Am.*, 90(6): 1353–1368.

Wang Xiaofeng, Feng Mei, Shi Danian, Ma Yinsheng, Chen Xuanhua, Ou Mingyi, Huo Guanghui, Wang Lianqing, Tian Xiaojuan, Zhang Xijuan, Li Huijun, Li Guoqi and Jiang Rongbao, 2006. Application of the Passive Seismic Tomography Method to Deep Tectonics Study in Oil Field. *Geol. Bull. China*, 25(9–10): 1028–1031 (in Chinese with English abstract).

Wessel, P., and Smith W.H.F., 1991. Free software helps map and display data. *EOS Trans. AGU.*, 72: 411.

Xu Yi , Liu Futian , Liu Jianhua and Chen Hui, 2002. Crust and upper mantle structure beneath western China from P wave travel time tomography. *J. Geophys. Res.*, 107(B10): 2220.

Zhang Peizhen, Shen Zhengkang, Wang Min, Gan Weijun, Bürgmann, R., Molnar, P., Wang Qi, Niu Zhijun, Sun Jianzhong, Wu Jianchun, Hanrong Sun and Xinzhao You, 2004. Continuous deformation of the Tibetan Plateau from global positioning system data. *Geology*, 32(9): 809–812.

Zhao Zhu, Fan Jun, Zheng Si Hua, Hasegawa, A. and Horiuchi, S., 1997. Crustal structure and accurate hypocenter determination along the Longmenshan fault zone. *Acta Seismologica Sinica*, 10(6): 761–768.

Zhou Huawei and Murphy, M.A., 2005. Tomographic evidence for wholesale underthrusting of India beneath the entire Tibetan plateau. *J. Asian Earth Sci.*, 25(3): 445–457.